nature genetics

Biallelic mutations in human *DCC* cause developmental split-brain syndrome

Saumya S Jamuar[1–5,22], Klaus Schmitz-Abe[1,2,4,22], Alissa M D'Gama[1,4,5], Marie Drottar[6], Wai-Man Chan[5–8], Maya Peeva[6–8], Sarah Servattalab[1,4,5], Anh-Thu N Lam[1,4,5], Mauricio R Delgado[9,10], Nancy J Clegg[9], Zayed Al Zayed[11], Mohammad Asif Dogar[12], Ibrahim A Alorainy[13], Abdullah Abu Jamea[13], Khaled Abu-Amero[14], May Griebel[15], Wendy Ward[15], Ed S Lein[16], Kyriacos Markianos[1,2,4,17], A James Barkovich[18], Caroline D Robson[19], P Ellen Grant[6,19], Thomas M Bosley[20], Elizabeth C Engle[1,4,5–8,21], Christopher A Walsh[1,2,4,5,7,21] & Timothy W Yu[1,2,21]

Motor, sensory, and integrative activities of the brain are coordinated by a series of midline-bridging neuronal commissures whose development is tightly regulated. Here we report a new human syndrome in which these commissures are widely disrupted, thus causing clinical manifestations of horizontal gaze palsy, scoliosis, and intellectual disability. Affected individuals were found to possess biallelic loss-of-function mutations in the gene encoding the axon-guidance receptor 'deleted in colorectal carcinoma' (*DCC*), which has been implicated in congenital mirror movements when it is mutated in the heterozygous state but whose biallelic loss-of-function human phenotype has not been reported. Structural MRI and diffusion tractography demonstrated broad disorganization of white-matter tracts throughout the human central nervous system (CNS), including loss of all commissural tracts at multiple levels of the neuraxis. Combined with data from animal models, these findings show that *DCC* is a master regulator of midline crossing and development of white-matter projections throughout the human CNS.

Commissural neurons are responsible for bridging the left and right halves of the central nervous system and have been hypothesized to account for the emergence of key neurobiological features during vertebrate evolution, such as depth perception and locomotion. Disruption of subsets of brain commissures occurs in a number of human syndromes: in the forebrain, agenesis of the corpus callosum (ACC), the largest commissural tract in the human brain, may be present as an isolated feature or in combination with other malformations (for example, holoprosencephaly)[1–4], with or without intellectual disability. In the brainstem, disruption of midbrain and pontine commissural tracts is a key feature of the genetic syndrome horizontal gaze palsy with progressive scoliosis (HGPPS; Online Mendelian Inheritance in Man (OMIM) 607313), owing to biallelic mutations in *ROBO3* (OMIM 608630))[5]. Individuals with HGPPS exhibit abnormalities of conjugate eye movement and early-onset scoliosis, but normal intellect. In this report, we describe a new human genetic syndrome that combines features of ACC with HGPPS. Affected individuals exhibit clinical manifestations of horizontal gaze palsy, intellectual disability, and scoliosis (**Fig. 1** and **Supplementary Fig. 1**). We traced the cause of this syndrome to biallelic mutations in the axon-guidance receptor–encoding gene *DCC* (OMIM 120470)), which has previously been implicated, via heterozygous mutations, in congenital mirror movements[6–8] but whose human knockout phenotype has not been described.

Family 1 is from Mexico and includes two boys exhibiting a constellation of neurological abnormalities, including horizontal gaze

[1]Division of Genetics and Genomics, Boston Children's Hospital, Boston, Massachusetts, USA. [2]Department of Pediatrics, Harvard Medical School, Boston, Massachusetts, USA. [3]Department of Paediatrics, KK Women's and Children's Hospital, Paediatric Academic Clinical Programme, Duke–NUS Medical School, Singapore. [4]Manton Center for Orphan Disease Research, Boston Children's Hospital, Boston, Massachusetts, USA. [5]Howard Hughes Medical Institute, Boston Children's Hospital, Boston, Massachusetts, USA. [6]Fetal-Neonatal Neuroimaging and Developmental Science Center, Division of Newborn Medicine, Boston Children's Hospital, Boston, Massachusetts, USA. [7]Department of Neurology, Boston Children's Hospital and Harvard Medical School, Boston, Massachusetts, USA. [8]Department of Ophthalmology, Boston Children's Hospital and Harvard Medical School, Boston, Massachusetts, USA. [9]Department of Neurology, Texas Scottish Rite Hospital for Children, Dallas, Texas, USA. [10]Department of Neurology and Neurotherapeutics, University of Texas Southwestern Medical Center at Dallas, Dallas, Texas, USA. [11]Department of Orthopedic Surgery, King Faisal Specialist Hospital and Research Centre, Riyadh, Saudi Arabia. [12]Imaging Institute, Cleveland Clinic, Abu Dhabi, United Arab Emirates. [13]Department of Radiology, King Saud University, Riyadh, Saudi Arabia. [14]Department of Ophthalmology, King Saud University, Riyadh, Saudi Arabia. [15]Department of Pediatrics and Neurology, Arkansas Children's Hospital and University of Arkansas for Medical Sciences, Little Rock, Arkansas, USA. [16]Allen Institute for Brain Science, Seattle, Washington, USA. [17]Department of Pathology, Harvard Medical School, Boston, Massachusetts, USA. [18]Department of Radiology and Biomedical Imaging, University of California, San Francisco, San Francisco, California, USA. [19]Department of Radiology, Boston Children's Hospital and Harvard Medical School, Boston, Massachusetts, USA. [20]The Wilmer Eye Institute, Johns Hopkins University, Baltimore, Maryland, USA, and Department of Ophthalmology, College of Medicine, King Saud University, Riyadh, Saudi Arabia. [21]Program in Medical and Population Genetics, Broad Institute of Massachusetts Institute of Technology (MIT) and Harvard, Cambridge, Massachusetts, USA. [22]These authors contributed equally to this work. Correspondence should be addressed to T.W.Y. (timothy.yu@childrens.harvard.edu).

Received 22 June 2016; accepted 3 February 2017; published online 27 February 2017; doi:10.1038/ng.3804

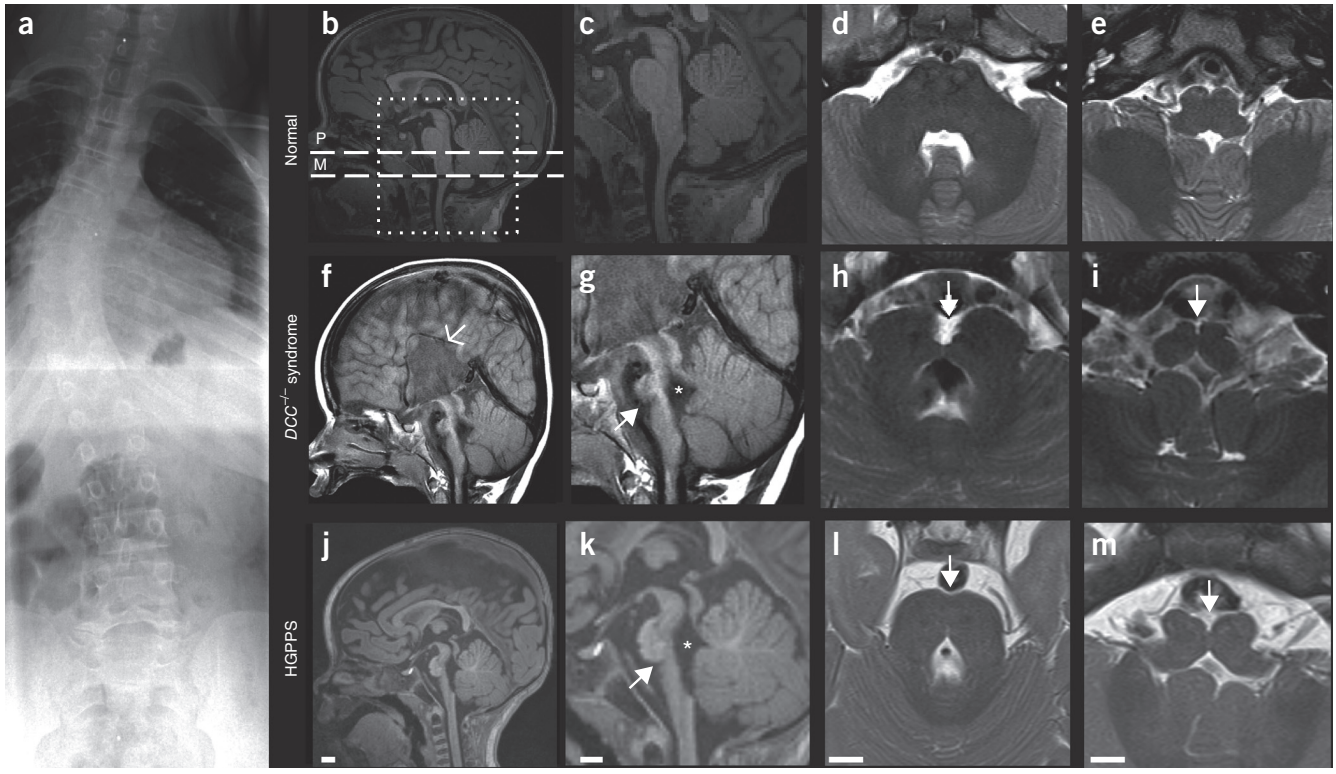

Figure 1 Radiographic features of the *DCC*$^{-/-}$ syndrome. (**a**) Spine film from individual II:7 from family 1, showing thoracolumbar scoliosis. (**b**–**m**) MRI brain features of affected individual II:2 from family 2 compared with an age-matched control and an individual with horizontal gaze palsy and progressive scoliosis (HGPPS). (**b**,**f**,**j**) Sagittal images showing agenesis of the corpus callosum (arrow) and absent anterior commissure in the affected individual but an intact corpus callosum in control and HGPPS individuals. (**c**,**g**,**k**) Enlargement (boxed area in **b**) of the sagittal image, showing brainstem abnormalities. Asterisks denote an enlarged fourth ventricle. The pons is hypoplastic (arrow) in both affected and HGPPS individuals, but especially in *DCC*$^{-/-}$ individuals, and there is associated elongation of the midbrain and medulla. All are dysmorphic, particularly the pons and midbrain with midline cleft, compared with the control. (**d**,**h**,**l**) Axial images through the pons (dashed line 'P' in **b**), showing hypoplasia of the pons and middle cerebellar peduncle and the cleft in the brainstem in the affected and HGPPS individuals (arrow). In addition, the anterior surface of the pons appears irregular. (**e**,**i**,**m**) Axial images through the medulla (dashed line 'M' in **b**), showing hypoplasia and a 'butterfly' appearance of the medulla in the affected and HGPPS individuals (arrow). Scale bars, 1 cm.

palsy, intellectual disability, and progressive scoliosis (**Fig. 2a**, **Supplementary Table 1**, and **Supplementary Note**). Brain magnetic resonance imaging (MRI) identified several abnormalities in the affected individuals (**Fig. 1**, **Supplementary Table 1**, and **Supplementary Fig. 1**), including ACC and an absence of the anterior and hippocampal commissures. The massa intermedia was slightly large, possibly indicative of partial fusion of the thalamus, although normal variation could not be excluded. The pons and midbrain structures were hypoplastic, and there was a large midline cleft throughout the extent of the brainstem, thus contributing to a butterfly-shaped medulla (**Supplementary Table 1** and **Supplementary Fig. 1b**–**g**).

Family 2 is from Saudi Arabia. The parents are first cousins who have a daughter affected with horizontal gaze palsy, developmental delay, and progressive scoliosis (**Fig. 2b**, **Supplementary Table 1**, and **Supplementary Note**). MRI of the daughter's brain demonstrated ACC and a large midline cleft of the brainstem (**Fig. 1f**–**i**), resembling the abnormalities seen in family 1.

Homozygosity mapping in family 1 identified a large 23-cM block of homozygosity on chromosome 18 that was shared by both affected individuals (**Supplementary Fig. 2a**). Copy-number variation (CNV) analysis demonstrated that this region contained two homozygous deletions of ~36 kb and ~7 kb at 18q12.3 and 18q21.2, respectively (**Supplementary Fig. 3**). The 18q12.3 deletion did not overlap any known genes and is a site of frequent CNV in the population (Database of Genomic Variants (DGV) esv2421793; deletion observed in 1.5% of HapMap samples). In contrast, the 7-kb 18q21.2 deletion was found to be absent from public or internal databases, and was predicted to lie within the gene *DCC* (**Supplementary Fig. 3**). *DCC* encodes a 1,447–amino acid cell-surface receptor with four immunoglobulin and six fibronectin type III repeats, a transmembrane domain, and an intracellular domain[9]. DCC is a receptor for Netrin[10], a diffusible guidance cue expressed at the CNS midline; together, DCC and Netrin constitute key members of a signaling pathway for axon guidance that is evolutionarily conserved in vertebrates and *Caenorhabditis elegans*[11]. In humans, heterozygous mutations in *DCC* have been shown[6] to cause congenital mirror movements (CMM/MRMV1; OMIM 157600)), an autosomal-dominant condition in which intentional movements on one side of the body are accompanied by involuntary pathological movements on the opposite side. Beyond these mirror movements, described patients with heterozygous *DCC* mutations are otherwise neurotypical, lacking neurocognitive symptoms, eye-movement abnormalities, scoliosis, or brain malformations. To our knowledge, no patients with biallelic mutations in *DCC* have been described to date.

Digital droplet PCR confirmed the homozygous *DCC* deletion in both affected boys. Their mother is a heterozygous carrier, and their father was unavailable for analysis (**Supplementary Fig. 4a**). We used a series of PCR probes (**Supplementary Fig. 4b**) to localize the precise

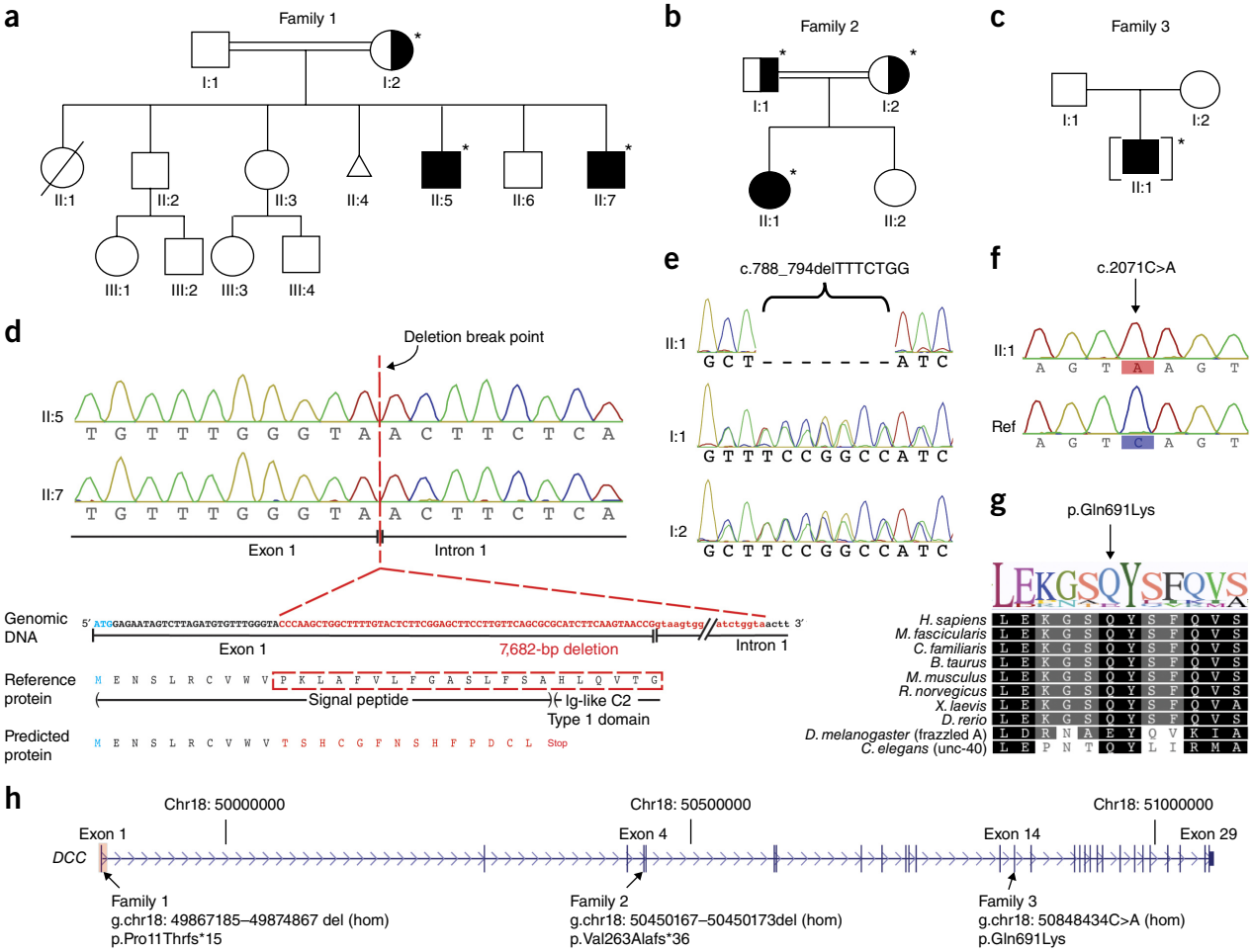

Figure 2 Identification of biallelic mutations in *DCC*. (**a**–**c**) Pedigrees of families 1 (**a**), 2 (**b**), and 3 (**c**). Asterisks indicate family members whose DNA was available. (**d**) Sequencing of the junction PCR products in family 1 confirmed a 7,682-bp intragenic deletion (red; chromosome (chr) 18: 49867184–49874866, hg19 coordinates) that is predicted to result in deletion of 21 amino acids (dashed red box) from the DCC protein, including part of the signal peptide, the Ig-like C2-type 1 domain and the exon 1–intron 1 splice junction. The predicted amino acid sequence also leads to a premature stop codon 15 amino acids downstream of the first changed amino acid. ATG/M (blue), translation start site for the predominant isoform of *DCC* (NM_005215.3). (**e**) Sanger traces from *DCC* sequencing in family 2 identified a homozygous out-of-frame 7-bp deletion in exon 4 (c.788_794delTTTCTGG) in the proband and a heterozygous deletion in the parents. (**f**) Sanger trace from *DCC* sequencing in family 3 identified the homozygous missense variant (NM_005215.3) c.2071C>A; p.Gln691Lys. (**g**) The glutamine residue at position 691 is a highly conserved residue in *Homo sapiens*, *Macaca fascicularis*, *Canis familiaris*, *Bos taurus*, *Mus musculus*, *Rattus norvegicus*, *Xenopus laevis*, *Danio rerio*, and *C. elegans*, with the exception of frazzled in *Drosophila melanogaster,* which is known to be significantly divergent from other orthologs. (**h**) Schematic of the *DCC* exon–intron structure, with locations of the mutations in the three families shown. Hom, homozygous.

breakpoint (**Supplementary Fig. 4c**), identifying a 7,682-bp deletion (**Fig. 2d**). This deletion removed the 3′ end of exon 1, containing 61 bp of *DCC* coding sequence (NM_005215.3) and 7.6 kb of intronic sequence (**Fig. 2d**,**h**). RT–PCR from patient lymphoblasts demonstrated that this deletion causes exon 1 to be skipped entirely (**Supplementary Fig. 5a**–**c**). Exon 1 is the first coding exon and contains the signal peptide, which is required for correct orientational insertion into the membrane, and part of the first of DCC's four immunoglobulin repeats, which adopt a horseshoe configuration critical for Netrin-mediated guidance[12]. Disruption of these features strongly suggests that this mutation represents a functional null.

Targeted sequencing of *DCC* in the proband of family 2 identified a homozygous 7-bp deletion in exon 4 (c.788_794delTTTCTGG) (**Fig. 2e**). Both parents are carriers. This variant is absent from public databases (Exome Aggregation Consortium, Exome Variant Server, dbSNP146, and the 1000 Genomes Project) as well as an internal exome database of >1,000 samples from Middle Eastern individuals. It is located at amino acid position 263 (of 1,447) in the third immunoglobulin repeat and results in frameshift and premature termination 36 amino acids downstream (p.Val263Alafs*36).

We sequenced coding regions of *DCC* in 33 additional patients who exhibited abnormalities of the corpus callosum but who were not known to have horizontal gaze palsy or scoliosis. Only a few heterozygous missense changes of uncertain importance were detected, and the four patients involved were subsequently found to have plausible alternative explanations for their callosal abnormalities (**Supplementary Table 2**). No additional biallelic coding mutations were found (**Supplementary Table 2**), thus indicating that biallelic mutations in *DCC* are not common causes of ACC, in general. *DCC* sequencing in a cohort of 31 patients with ACC plus interhemispheric cyst did identify one individual (family 3, individual II:1; **Fig. 2c**, **Supplementary Table 1**, and **Supplementary Note**) with a homozygous missense variant (c.2071C>A, p.Gln691Lys) (**Fig. 2f**) affecting the third fibronectin repeat. In a previously

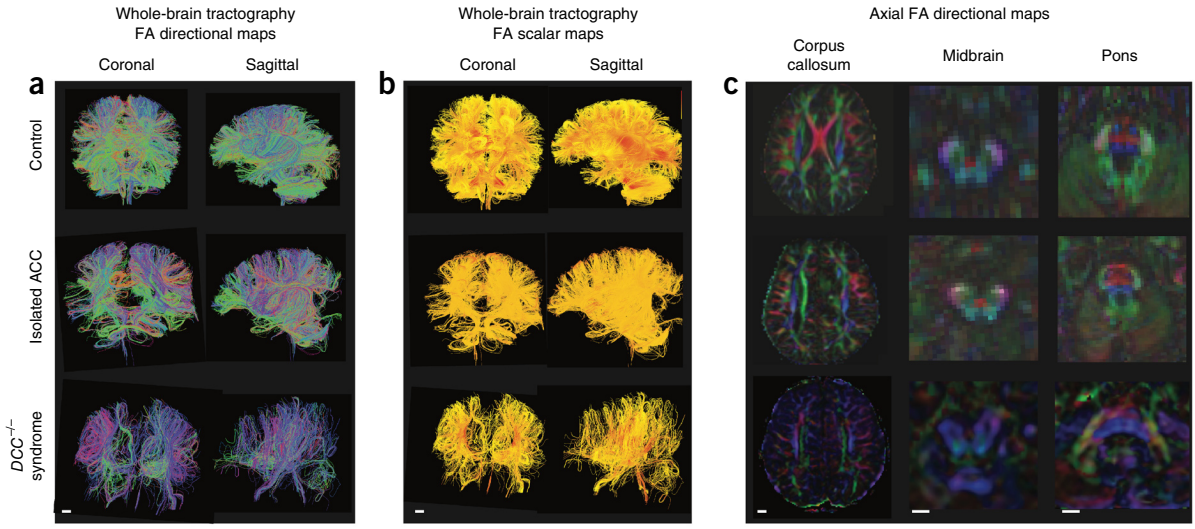

Figure 3 Axon-guidance defects in patients with *DCC*$^{-/-}$ syndrome. (**a**,**b**) Whole-brain diffusion tensor tractography (DTT) of a control individual, an individual with isolated agenesis of the corpus callosum, and an individual with *DCC*$^{-/-}$ syndrome. (**a**) Directional map tracts are pseudocolored to visualize the directions of anisotropic diffusion. Green tracts are in an anterior-to-posterior direction, red tracts are commissural tracts and blue tracts visualize inferior-to-superior tract directions. Both individuals with ACC and *DCC*$^{-/-}$ demonstrate absence of normal interhemispheric commissural fibers. In addition, the *DCC*$^{-/-}$ brain exhibits a paucity of reconstructable tracts. (**b**) Color scalar fractional anisotropy (FA) map, with a fractional direction scale with units from 0 to 1. A score of 0 (yellow) denotes fibers with relatively isotropic diffusion; a score of 1 (red) denotes fibers with more anisotropic diffusion. Fibers in the *DCC*$^{-/-}$ brain exhibit lower anisotropy, and the fibers appear generally disorganized, as compared with fibers in the control and isolated ACC individuals. (**c**) Axial FA directional maps of human brains at the levels of the corpus callosum, midbrain, and pons. Both ACC and *DCC*$^{-/-}$ brains lack normal crossing fibers (red). In addition, in control and ACC individuals, midbrain color FA maps demonstrate a distinctive red-dot sign denoting midline decussation of fibers of the superior cerebellar peduncle, which are absent from the *DCC*$^{-/-}$ brain. Similarly, in the pons, control and ACC individuals exhibit distinct crossing fibers representing midline crossing pontocerebellar fibers; these fibers are also absent in the *DCC*$^{-/-}$ individual. Scale bars, 1 cm.

published description[13], this male individual (patient 8) was noted to have ACC, an interhemispheric cyst, and modest intellectual deficits. No information about eye-movement abnormalities, mirror movements, or scoliosis was available, and the patient was unfortunately not available for recontact. This variant is not found in public allele-frequency databases, nor have any other variants affecting this amino acid position been reported. p.Gln691Lys alters a highly conserved glutamine residue in the third fibronectin type III domain (**Fig. 2g**), and this change was predicted to be deleterious by five of seven algorithms applied (**Supplementary Tables 3** and **4**). This finding suggests that weaker biallelic mutations in *DCC* may cause milder phenotypes, although additional cases will be required to confirm this possibility.

Diffusion MRI was available for the affected individual from family 2. We therefore performed diffusion tractography to reconstruct white-matter tracts from this individual. In age-matched control individuals, whole-brain tractography and fractional anisotropy maps showed a highly organized network of fibers, which were distinguishable as associational (cortical–cortical projections), commissural (interhemispheric projections), and subcortical (descending projections) fibers. In contrast, tractography of the *DCC*$^{-/-}$ brain showed striking abnormalities (**Fig. 3**, **Supplementary Figs. 6** and **7**, and **Supplementary Videos 1–6**). In place of the normal pattern of interdigitating callosal fibers, no commissural tracts were evident in either tractography or fractional anisotropy maps (**Fig. 3a**,**b** and **Supplementary Fig. 7a**). *DCC*$^{-/-}$ reconstructions did show characteristic longitudinally misguided Probst bundles along the lateral ventricles (**Supplementary Fig. 7b**), a common finding in some individuals with agenesis of the corpus callosum[14]. White-matter tracts in the *DCC*$^{-/-}$ mutant brain were much more disorganized than those in control individuals (**Fig. 3a**,**b** and **Supplementary Fig. 7a**). Fewer fibers were able to be reconstructed, and the reconstructed tracts showed much lower anisotropy, a measure of axonal integrity and myelination (**Fig. 3a**,**b** and **Supplementary Fig. 6**). This effect was not limited to commissural fibers but was also strongly evident in associational and subcortical fibers. Fractional anisotropy maps pseudocolored for directionality (**Fig. 3a**,**b**) suggested that the *DCC*$^{-/-}$ brain is especially depleted of associational fiber bundles (for example, projecting longitudinally or anterior–posterior, in green), and fibers are instead predominantly arranged in a radial fashion (for example, dorsal–ventral, in blue). In comparison, whole-brain tractography of an individual with idiopathic agenesis of the corpus callosum (**Fig. 3a**,**b** and **Supplementary Fig. 6**) did not show similar disorganization, decreased fiber number, or low anisotropy, thus suggesting that these are neuroanatomic features specific to disruption of *DCC*.

Individuals with HGPPS do not exhibit ACC but have been shown to have distinctive crossing abnormalities in the brainstem, including the absence of major pontine crossing fiber tracts and the lack of decussation of the superior cerebellar peduncles in the midbrain[15]. Color fractional anisotropy maps from our *DCC*$^{-/-}$ patient showed a similar failure of superior cerebellar peduncles to decussate, as evidenced by the absence of the typical midbrain 'red dot' sign[16] (**Fig. 3c**). In the pons, our patient had small middle-cerebellar peduncles and also lacked evidence of transverse pontine fibers (**Fig. 3c**), similarly to individuals with HGPPS.

Heterozygous mutations in *DCC* in humans have been associated with CMM[6–8] and include several early truncating mutations, thus suggesting that the relevant underlying mechanism is loss of

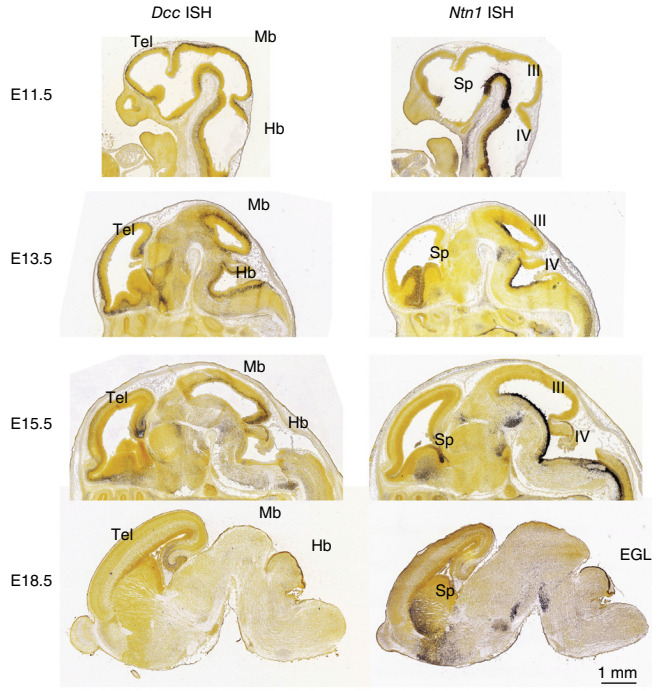

Figure 4 Expression patterns of *Dcc* and *Ntn1* in the developing brain. *In situ* hybridization (ISH) patterns in mice at embryonic day (E) 11.5, E13.5, E15.5, and E18.5, showing robust early expression in specific, yet largely complementary, cell populations in the developing telencephalon (Tel), midbrain (Mb) and hindbrain (Hb). *Dcc* is particularly highly expressed at early stages in developing neurons of the cortical plate and brainstem nuclei; *Dcc* expression subsequently tapers off with age. Similarly, *Ntn1* expression is highest in midline structures of the telencephalic expansion and the ventral floor of the developing third (III) and fourth (IV) ventricles; its expression also becomes much broader as development proceeds. Sp, subpallium; EGL, external granule layer of the cerebellum.

function via haploinsufficiency. The *DCC* mutations described in this report were also predicted to be associated with a loss of function, but none of the heterozygous carriers (that were able to be assessed) were reported to exhibit mirror movements. Furthermore, whereas the proband in family 1 exhibited mirror movements, the affected individuals in family 2 and 3 did not. The reason for this variability is unclear, but incomplete penetrance has also been observed in CMM[6], and it is possible that this phenotype may be influenced by additional yet-uncharacterized background genetic-modifier effects. It is also possible that involuntary mirror movements require a particular mix of contralateral and ipsilateral connectivity, owing to partial loss of *DCC* function (for example, heterozygous knockout), that might be lacking in a complete knockout. We note, for example, that individuals with biallelic *ROBO3* mutations exhibit uncrossed ascending sensory and descending motor pathways, and also lack mirror movements.

In the embryonic mouse brain, *DCC* is highly expressed in the telencephalic cortical plate as well as in developing brainstem nuclei[10] (**Fig. 4**). Netrin-1 (*Ntn1*) is expressed in ventral midline structures of the developing forebrain and the third and fourth ventricles[17] (**Fig. 4**), and similar findings have recently been reported in postmortem human fetal tissue[18]. The forebrain crossing deficits observed in our patients are reminiscent of abnormalities previously reported in mouse knockout models of Netrin-1 or DCC deficiency, which are also acallosal[19–21]. This observation is thought to be due to a failure of DCC signaling in pioneering commissural axons from the cingulate and neocortex[22,23]. Crossing deficits in the brainstem have been less consistently predicted from animal studies, although zebrafish DCC mutants show hindbrain startle-circuit abnormalities, and tract positioning defects have been observed in mice[22,23]. Animal studies have also implicated DCC in the formation of a wide variety of additional axon tracts, including corticospinal tract development in mice[21], axon guidance in the olfactory bulb[24], and patterning of thalamocortical projections[25,26]. DCC and Netrin-1 have also been shown to play roles in oligodendrocyte myelin regulation[27,28], thus potentially contributing to the loss of tract fiber integrity in DTI imaging observed herein.

The human *DCC*-knockout phenotype appears to unify major clinical and neuroimaging features of three separate disorders of axon guidance: ACC, HGPPS, and CMM (previously associated with heterozygous mutations in *DCC*[6]) (**Fig. 5**). Individuals with $DCC^{-/-}$ mutations have brainstem flattening/midline clefting and eye-movement abnormalities similar to those seen in HGPPS[5,14], thus reflecting shared brainstem crossing defects that disrupt pathways controlling conjugate gaze. These individuals also share progressive scoliosis, the cause of which is less well understood. We speculate that scoliosis may pertain to unbalanced paraspinal muscle activity due to defective spinal interneuron circuits (required for coordination of left–right locomotory patterns), because these circuits have been shown to be disrupted in Netrin-1- and DCC-deficient mice[29,30]. Intellectual disability is not seen in HGPPS, but it can (though not always) accompany ACC[31]. Our patients' cognitive deficits may be at least partially attributable to noncommissural forebrain white-matter abnormalities as well.

The overlap of the human *DCC*-knockout phenotype with HGPPS is mechanistically important. HGPPS is caused by mutations in the *ROBO3* gene, which encodes an axon-guidance receptor known to interact molecularly and functionally with DCC[32]. *ROBO3* is a divergent mammalian homolog of the genes encoding the roundabout (Robo) receptor in *C. elegans*, *Drosophila*, and zebrafish[33] . It is expressed by commissural axons of the spinal cord and hindbrain, and is required for hindbrain–axon midline crossing[5]. Unlike other Robo receptors, Robo3 does not bind with high affinity to Slits and hence does not mediate repulsion of neurons away from the midline. Instead, Robo3 forms a direct molecular complex with DCC that silences repulsion from Slits[33] (thus allowing developing neurons to approach) and enhances attraction to Netrins[33,34]. The similarities in the brainstem phenotypes in HGPPS and the $DCC^{-/-}$ patients reported here provides strong evidence that this functional hierarchy is also conserved in humans.

In summary, this is, to our knowledge, the first report of human biallelic mutations in *DCC* in association with a new genetic syndrome of horizontal gaze palsy, scoliosis, ACC, and midline brainstem cleft. Our data demonstrate that *DCC* is essential for both forebrain and brainstem midline crossing in the human CNS. According to our findings, we recommend screening individuals with horizontal gaze palsy, scoliosis, ACC, and midline brainstem malformations for mutations in *DCC*. Strong consideration should also be given to other genes in the Netrin–DCC pathway as candidate genes. Further delineation of the developmental consequences of mutations in this pathway should help shed light on the evolution of bilateral symmetry in the human nervous system.

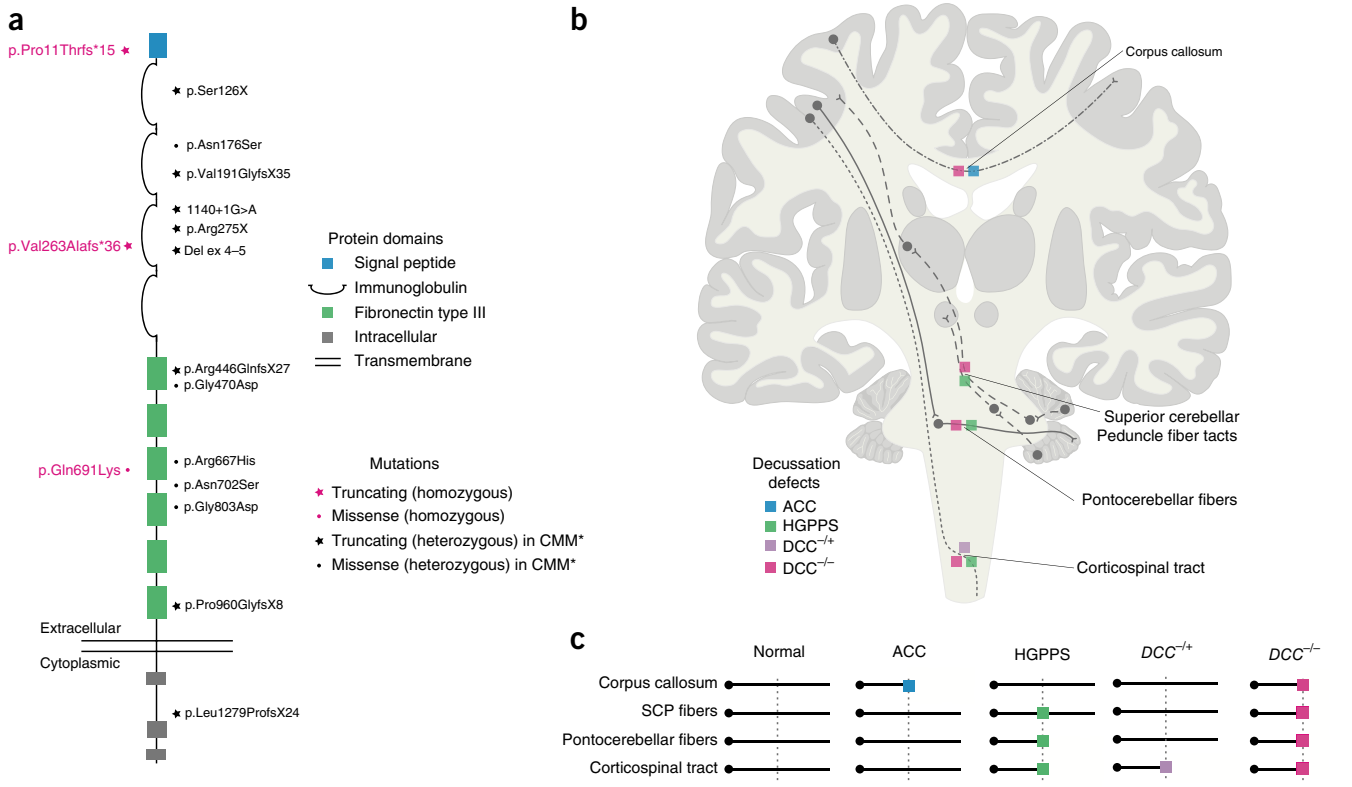

Figure 5 Genotype–phenotype correlations in *DCC* and other related disorders of midline axon guidance. (**a**) Structure of the DCC protein and location of the *DCC* mutations identified here (magenta) and in congenital mirror movements (black). *DCC* encodes a transmembrane receptor with four immunoglobulin and six fibronectin type III domains, and three conserved cytoplasmic domains. In family 1, homozygous loss of exon 1 results in a deletion of the signal peptide as well as the first immunoglobulin-like C2 domain and is predicted to result in a nonfunctional protein. In family 2, homozygous frameshift in exon 4 is predicted to result in a nonfunctional protein. In family 3, the missense mutation (p.Gln691Lys) affects the third fibronectin type III domain. Individuals with congenital mirror movements have truncating or missense heterozygous mutations in *DCC*; however, these individuals have normal brain MRI and normal intellect. Asterisk denotes references 6–8. (**b**,**c**) Major tract abnormalities in $DCC^{-/-}$ syndrome and other human disorders of axon guidance. Anatomical schematic comparing ACC (blue box), HGPPS (green box), $DCC^{+/-}$ (purple box), and $DCC^{-/-}$ (magenta box) phenotypes (**b**), and summary schematic (**c**) depicting disruptions in different commissural tracts in each disorder. In ACC, only supratentorial tracts are affected, whereas in HGPPS, only infratentorial tracts are affected. In $DCC^{+/-}$, corticospinal tracts are functionally disrupted. In $DCC^{-/-}$, midline crossing along the entire length of the neuraxis is disrupted. ACC, agenesis of corpus callosum; HGPPS, horizontal gaze palsy with progressive scoliosis.

URLs. TrackVis.org, http://trackvis.org.

METHODS

Methods, including statements of data availability and any associated accession codes and references, are available in the online version of the paper.

Note: Any Supplementary Information and Source Data files are available in the online version of the paper.

ACKNOWLEDGMENTS

We thank A. Rozzo, J. Partlow, B. Barry, and R. Hill for logistical and administrative assistance; C. Carruthers, research assistant in FNNDSC, for creating and compressing the DTT movie files; and H. Somhegyi for expert illustrations. We thank the individuals and their families reported on herein for their participation in this research. This research was supported in part by the Repository Core for Neurological Disorders, Department of Neurology, Boston Children's Hospital, and the IDDRC (NIH P30HD018655). S.S.J. is supported by the National Medical Research Council, Singapore, and the Singhealth-Duke NUS Paediatric Academic Programme Nurturing Clinician Scientist Scheme. A.M.D. is supported by the National Institute of General Medical Sciences (T32GM07753) and a National Institutes of Health Ruth L. Kirschstein National Research Service Award (5T32 GM007226-39). E.C.E.'s contributions to this work were supported by NEI R01EY12498, IDDRC grant P30 HD018655, and the Manton Center for Orphan Disease Research. C.A.W. is supported by grants from the National Institute of Mental Health (R01MH083565), the National Institute of Neurological Disorders and Stroke (R01NS032457 and R01NS035129), the Simons Foundation, and the Manton Center for Orphan Disease Research. C.A.W. and E.C.E. are supported as Investigators of the Howard Hughes Medical Institute. T.W.Y.'s contributions to this work were supported by grants from the National Institute of Mental Health (R01MH083565), the Simons Foundation, and the Nancy Lurie Marks Foundation.

AUTHOR CONTRIBUTIONS

S.S.J., E.C.E., C.A.W., and T.W.Y. designed experiments. K.S.-A. and K.M. performed the homozygosity and CNV analysis. S.S.J., A.M.D., A.-T.N.L., and S.S. performed the ddPCR, junction PCR, and RT–PCR. W.-M.C. performed Sanger sequencing of family 2. M.P., M.D., and P.E.G. performed the DTI and tractography analyses. M.R.D., N.J.C., M.G., Z.A.Z., M.A.D., A.A.J., K.A.-A., and T.M.B. performed the phenotypic assessment of the patients. A.J.B., C.A.W., M.D., M.P., C.D.R., I.A.A., P.E.G., E.C.E., and T.W.Y. reviewed the MRI imaging studies. W.W. performed the phenotypic assessment of patient 3, and E.S.L. performed the *in situ* hybridization analyses. S.S.J., E.C.E., C.A.W., and T.W.Y. wrote the manuscript. All coauthors reviewed and approved the final version of the submitted manuscript.

COMPETING FINANCIAL INTERESTS

The authors declare competing financial interests: details are available in the online version of the paper.

1. Edwards, T.J., Sherr, E.H., Barkovich, A.J. & Richards, L.J. Clinical, genetic and imaging findings identify new causes for corpus callosum development syndromes. *Brain* **137**, 1579–1613 (2014).
2. Izzi, L. & Charron, F. Midline axon guidance and human genetic disorders. *Clin. Genet.* **80**, 226–234 (2011).
3. Nugent, A.A., Kolpak, A.L. & Engle, E.C. Human disorders of axon guidance. *Curr. Opin. Neurobiol.* **22**, 837–843 (2012).
4. Van Battum, E.Y., Brignani, S. & Pasterkamp, R.J. Axon guidance proteins in neurological disorders. *Lancet Neurol.* **14**, 532–546 (2015).
5. Jen, J.C. *et al.* Mutations in a human ROBO gene disrupt hindbrain axon pathway crossing and morphogenesis. *Science* **304**, 1509–1513 (2004).
6. Srour, M. *et al.* Mutations in *DCC* cause congenital mirror movements. *Science* **328**, 592 (2010).
7. Depienne, C. *et al.* A novel *DCC* mutation and genetic heterogeneity in congenital mirror movements. *Neurology* **76**, 260–264 (2011).
8. Méneret, A. *et al.* Congenital mirror movements: mutational analysis of *RAD51* and *DCC* in 26 cases. *Neurology* **82**, 1999–2002 (2014).
9. Kolodziej, P.A. *et al. frazzled* encodes a *Drosophila* member of the DCC immunoglobulin subfamily and is required for CNS and motor axon guidance. *Cell* **87**, 197–204 (1996).
10. Keino-Masu, K. *et al.* Deleted in Colorectal Cancer (DCC) encodes a netrin receptor. *Cell* **87**, 175–185 (1996).
11. Moore, S.W., Tessier-Lavigne, M. & Kennedy, T.E. Netrins and their receptors. *Adv. Exp. Med. Biol.* **621**, 17–31 (2007).
12. Chen, Q. *et al.* N-terminal horseshoe conformation of DCC is functionally required for axon guidance and might be shared by other neural receptors. *J. Cell Sci.* **126**, 186–195 (2013).
13. Griebel, M.L., Williams, J.P., Russell, S.S., Spence, G.T. & Glasier, C.M. Clinical and developmental findings in children with giant interhemispheric cysts and dysgenesis of the corpus callosum. *Pediatr. Neurol.* **13**, 119–124 (1995).
14. Wahl, M., Barkovich, A.J. & Mukherjee, P. Diffusion imaging and tractography of congenital brain malformations. *Pediatr. Radiol.* **40**, 59–67 (2010).
15. Sicotte, N.L. *et al.* Diffusion tensor MRI shows abnormal brainstem crossing fibers associated with *ROBO3* mutations. *Neurology* **67**, 519–521 (2006).
16. Kweldam, C.F. *et al.* Undecussated superior cerebellar peduncles and absence of the dorsal transverse pontine fibers: a new axonal guidance disorder? *Cerebellum* **13**, 536–540 (2014).
17. Serafini, T. *et al.* Netrin-1 is required for commissural axon guidance in the developing vertebrate nervous system. *Cell* **87**, 1001–1014 (1996).
18. Harter, P.N. *et al.* Spatio-temporal deleted in colorectal cancer (DCC) and netrin-1 expression in human foetal brain development. *Neuropathol. Appl. Neurobiol.* **36**, 623–635 (2010).
19. Fazeli, A. *et al.* Phenotype of mice lacking functional Deleted in colorectal cancer (*Dcc*) gene. *Nature* **386**, 796–804 (1997).
20. Fearon, E.R. *et al.* Identification of a chromosome 18q gene that is altered in colorectal cancers. *Science* **247**, 49–56 (1990).
21. Finger, J.H. *et al.* The netrin 1 receptors Unc5h3 and Dcc are necessary at multiple choice points for the guidance of corticospinal tract axons. *J. Neurosci.* **22**, 10346–10356 (2002).
22. Fothergill, T. *et al.* Netrin-DCC signaling regulates corpus callosum formation through attraction of pioneering axons and by modulating Slit2-mediated repulsion. *Cereb. Cortex* **24**, 1138–1151 (2014).
23. Srivatsa, S. *et al.* Unc5C and DCC act downstream of Ctip2 and Satb2 and contribute to corpus callosum formation. *Nat. Commun.* **5**, 3708 (2014).
24. Lakhina, V. *et al.* Netrin/DCC signaling guides olfactory sensory axons to their correct location in the olfactory bulb. *J. Neurosci.* **32**, 4440–4456 (2012).
25. Powell, A.W., Sassa, T., Wu, Y., Tessier-Lavigne, M. & Polleux, F. Topography of thalamic projections requires attractive and repulsive functions of Netrin-1 in the ventral telencephalon. *PLoS Biol.* **6**, e116 (2008).
26. Braisted, J.E. *et al.* Netrin-1 promotes thalamic axon growth and is required for proper development of the thalamocortical projection. *J. Neurosci.* **20**, 5792–5801 (2000).
27. Jarjour, A.A. *et al.* Maintenance of axo-oligodendroglial paranodal junctions requires DCC and netrin-1. *J. Neurosci.* **28**, 11003–11014 (2008).
28. Rajasekharan, S. *et al.* Netrin 1 and Dcc regulate oligodendrocyte process branching and membrane extension via Fyn and RhoA. *Development* **136**, 415–426 (2009).
29. Rabe, N., Gezelius, H., Vallstedt, A., Memic, F. & Kullander, K. Netrin-1-dependent spinal interneuron subtypes are required for the formation of left-right alternating locomotor circuitry. *J. Neurosci.* **29**, 15642–15649 (2009).
30. Rabe Bernhardt, N. *et al.* DCC mediated axon guidance of spinal interneurons is essential for normal locomotor central pattern generator function. *Dev. Biol.* **366**, 279–289 (2012).
31. Paul, L.K. *et al.* Agenesis of the corpus callosum: genetic, developmental and functional aspects of connectivity. *Nat. Rev. Neurosci.* **8**, 287–299 (2007).
32. Jen, J. *et al.* Familial horizontal gaze palsy with progressive scoliosis maps to chromosome 11q23-25. *Neurology* **59**, 432–435 (2002).
33. Sabatier, C. *et al.* The divergent Robo family protein rig-1/Robo3 is a negative regulator of slit responsiveness required for midline crossing by commissural axons. *Cell* **117**, 157–169 (2004).
34. Zelina, P. *et al.* Signaling switch of the axon guidance receptor Robo3 during vertebrate evolution. *Neuron* **84**, 1258–1272 (2014).

ONLINE METHODS

Standard protocol approval and patient consent. The families reported herein provided informed consent for their participation in this research, which was conducted according to protocols approved by the institutional review boards of Boston Children's Hospital and Beth Israel Deaconess Medical Center. No statistical method was used to predetermine sample size. The experiments were not randomized and were not performed with blinding.

SNP genotyping and copy-number analyses. DNA was extracted from blood with a DNeasy Blood and Tissue kit (Qiagen). Genome-wide SNP screening on the two affected individuals from family 1 was performed with Affymetrix 6.0 SNP Arrays. SNP genotyping data were used to perform homozygosity and copy-number analyses. Homozygosity mapping was performed as previously described[35]. CNV analysis was performed with four algorithms in parallel (Birdsuite, PennCNV, Nexus and Affymetrix Genotyping Console), requiring a minimum of ten probes and the concordance of at least two algorithms for specificity. To distinguish rare from common variation, results were matched against a catalog of reference CNVs generated via the same pipeline, by using 1,251 samples from the HapMap project (11 subpopulations, public release no. 3). For additional stringency, CNVs were further matched with CNVs present in the DGV as well as an internal database of CNVs from over 12,000 unrelated research samples (including >1,000 from individuals from the Middle East with a variety of neurodevelopmental conditions, and >105 healthy Saudi individuals).

CNV confirmation and characterization. CNV predictions were confirmed with digital qPCR with predesigned probes (Life Technologies) on a QX100 Droplet Digital PCR System (Bio-Rad). The boundaries of the deletion in family 1 were determined with staggered nested PCR primers (Integrated DNA Technologies) (**Supplementary Table 5**) spanning the predicted copy-number change (**Supplementary Fig. 3b**).

RT–PCR of patient cell lines. To further define the effects of this deletion in the *DCC* locus, we prepared RNA from lymphoblastoid cell lines generated from an affected individual and a healthy control individual (RNeasy Mini kit, Qiagen). cDNA was then prepared (SuperScript III Reverse Transcriptase, Life Technologies) and subjected to RT–PCR with primers (Integrated DNA Technologies) designed to target different exons of the predicted *DCC* mRNA transcript (**Supplementary Table 6**).

Sanger sequencing to identify additional families. We performed Sanger sequencing of *DCC* (RefSeq NM_005215.3) coding regions in 64 additional families with ACC with primers designed to target all 29 exons (**Supplementary Table 7**).

Magnetic resonance imaging and diffusion tensor tractography. MRI data for patient II:1 in family 2 were acquired on a 1.5T scanner (GE Signa HDxt. T1: TR, 500 ms; TE, 10 ms; voxel size, 0.7813 × 0.7813; slice thickness, 5 mm. DTI: TR/TE, 6,800/133 ms; b = 800 s/mm^2; b0 = 10; 25 gradient directions; in-plane resolution, 1.0156 × 1.0156; slice thickness, 5 mm, 27 slices). Patient imaging was compared with that of an age-matched female control and an age-matched female subject with agenesis of the corpus callosum (isolated ACC) but no *DCC* mutation (3.0T Siemens TrioTim. T1: TR, 2,530 ms; TE, 1.66 ms; 1-mm isotropic scan. DTI: TR/TE, 8000/104 ms; b = 1,000 s/mm^2; b0 = 10 (only one of which was used for subsequent analysis to match the patient data); 30 diffusion directions; in-plane resolution, 1.1724 × 1.1724; slice thickness, 5 mm; 28 slices). Before image postprocessing, the gradient directions (gd) in the control images and isolated ACC subject were downsampled from 30 gd to 25 gd to match the patient imaging.

Data analysis and interpretation were performed at Boston Children's Hospital. The diffusion data were postprocessed with the interpolated streamline algorithm in the Diffusion Toolkit developed at the Athinoula A. Martinos Center for Biomedical Imaging, Department of Radiology, Massachusetts General Hospital (Ruopeng Wang, Van J. Wedeen; TrackVis). Diffusion tensor estimation, fractional anisotropy metrics and fiber-tract reconstruction were performed with the standard linear least-squares fitting method. Fiber tracts were terminated either when the angle between two consecutive orientation vectors was greater than the given threshold of 45° or when fibers extended outside of the brain surface. The resulting tracts were displayed as either a directional fiber map or a scalar fractional anisotropy map on a 3D workstation. The color-coding of fibers was based on a standard RGB directional map and describes the fiber orientation. (red fibers, left–right; green fibers, anterior–posterior; blue fibers, superior–inferior). A whole-brain scalar image was also calculated for each case, with a fractional anisotropy scale from 0 to 1 and pseudocoloring from yellow to red. Yellow areas show isotropic diffusion, indicating more random water motion and less white-matter organization, whereas red areas show the diffusion anisotropy, as is normally seen along more organized (and probably myelinated) white-matter tracts. The scalar map describes the magnitude of the diffusion direction in the whole-brain tracts.

***In situ* hybridization (ISH).** ISH data were generated as part of the Allen Developing Mouse Brain atlas[36]. Briefly, a high-throughput ISH platform, as previously described in detail[37], was used to analyze transcript distributions for *Dcc* and *Ntn1* across four embryonic ages (E11.5, E13.5, E15.5, and E18.5 days postconception), with the following adaptations: (i) addition of the nuclear Feulgen–HP Yellow counterstain to allow for identification of anatomical structures and to enhance the ability to localize ISH signal; (ii) changes in the tissue embedding processes for embryonic tissue; (iii) adjustment of proteinase K concentrations optimized for each age; and (iv) adjustment of Nissl protocols for some time points. Slides were scanned with either the Image Capture System (ICS) platform developed for the Allen Mouse Brain Atlas[37] or a ScanScope automated slide scanner (Aperio Technologies) equipped with a 20× objective and Spectrum software, and whole-slide images were downsampled to a resolution of 1.0 μm/pixel. After imaging, individual section images were combined into a single slide image, and a tissue-detection algorithm assigned bounding boxes to individual tissue sections. A segmentation algorithm created the expression mask, which is provided as a colorized view of expression levels across the tissue[36].

Statistics. Formal statistical testing was not applicable for the results reported.

Data availability. Supporting genotype and DTI data from this study are available from the corresponding author upon request. Variant data from the families presented here have been deposited in ClinVar under accession numbers SCV000494148, SCV000494149, and SCV000494200.

35. Yu, T.W. *et al.* Mutations in *WDR62*, encoding a centrosome-associated protein, cause microcephaly with simplified gyri and abnormal cortical architecture. *Nat. Genet.* **42**, 1015–1020 (2010).
36. Thompson, C.L. *et al.* A high-resolution spatiotemporal atlas of gene expression of the developing mouse brain. *Neuron* **83**, 309–323 (2014).
37. Lein, E.S. *et al.* Genome-wide atlas of gene expression in the adult mouse brain. *Nature* **445**, 168–176 (2007).

 doi:10.1038/ng.3804